A Processive Single-Headed Motor: Kinesin Superfamily Protein KIF1A

Yasushi Okada, *et al.*

Science **283**, 1152 (1999);
DOI: 10.1126/science.283.5405.1152

A fast source of R^- rotons that enables this experiment to be performed has recently been developed (*13*). It is based on collisions between R^+ rotons as follows

$$R^+ + R^+ \rightarrow R^+ + R^- \qquad R^+ + R^+ \rightarrow R^- + R^- \qquad (4)$$

The source consists of two parallel metal films that form a narrow open-sided cavity containing liquid ^{4}He. The two metal films are heated simultaneously with a short pulse of current, injecting R^+ rotons and low-energy phonons into the cavity. R^- rotons are not injected by these heated films (*14*) but are created when the R^+ rotons interact. The pulse of R^+ and R^- rotons emitted from the cavity is short enough for time-of-flight measurements. This information gives an independent check that we are observing the effects of ballistic rotons and not spurious reflections.

To measure the quantum evaporation angle, the emitted rotons need to be collimated. We do this with horizontal semicircular slits so that the beam has the shape of the surface of a half cone. The source is ~9 mm below the liquid surface, and $\theta = 16.5°$ with a beam profile full width at half maximum of 7.5°. Atoms from R^- rotons should be refracted backward and converge several millimeters above the liquid surface, vertically above the source. This collimation arrangement enhances the R^- roton evaporation signal at a detector placed here (*15*). The detector can be moved horizontally so that the divergent beam of atoms from the R^+ rotons can also be detected for comparison.

The detector is 3 mm above the liquid surface. The energy deposited on the detector as a function of its horizontal position x (Fig. 2) is clearly composed of two separate components: maxima at $x \sim 0$ (directly above the roton source) and at $x \sim 6$ mm, with a minimum of almost zero at $x \sim 2.5$ mm. This spatial distribution of atoms is that expected from a beam containing R^- and R^+ rotons. The peak on the left comes from R^- rotons and the peak on the right from R^+ rotons. The times of flight support this identification. The result clearly shows the negative refraction of atom paths relative to R^- roton paths, thus demonstrating that the momentum and velocity of a R^- roton are antiparallel.

To make a quantitative comparison with theory we have made a computer simulation. A Monte Carlo procedure selects a roton from a thermal distribution at the source and follows it through the geometry of the collimation to the surface. An atom is liberated according to Eqs. 1 and 2, and a test is made of whether the atom hits the bolometer. For a roton spectrum with an effective temperature of 1 K, the simulation reproduces the main features of the measurements very well (Fig. 2). The remaining difference is most likely due to the evaporation probability being momentum dependent; in the simulation we took this probability to be constant because current theories of quantum evaporation do not agree on the momentum dependence (*16–18*).

We are only just beginning to understand the true nature of rotons. Now that beams of R^- rotons can be created, it should be possible to scatter them from R^+ rotons and probe their internal structure.

References and Notes

1. Assume that the kinetic energy ε as a function of momentum p of this hypothetical ball, mass m, is $\varepsilon = (p - p_0)^2/2m$ where $p_0 > 0$ and $0 < p < p_0$. The Newtonian racquet is assumed, as usual, to have a mass larger than that of the ball.
2. L. D. Landau, *J. Phys. Moscow* **11**, 91 (1947).
3. H. Palevsky, K. Otnes, K. E. Larsson, *Phys. Rev.* **112**, 11 (1958).
4. J. L. Yarnell, G. P. Arnold, P. J. Bendt, E. C. Kerr, *ibid.* **113**, 1379 (1959).
5. H. R. Glyde, M. R. Gibbs, W. G. Stirling, M. A. Adams, *Europhys. Lett.* **43**, 422 (1998).
6. W. G. Stirling, in *Proceedings of the Second Internal Conference on Phonon Physics*, J. Kollár, N. Kroó, N. Menyhárd, T. Siklós, Eds. (World Scientific, Singapore, 1985), pp. 829–835.
7. M. A. H. Tucker and A. F. G. Wyatt, *J. Low Temp. Phys.* **113**, 615 (1998).
8. P. W. Anderson, *Phys. Lett.* **29A**, 563 (1969).
9. M. W. Cole, *Phys. Rev. Lett.* **28**, 1622 (1972).
10. M. J. Baird, F. R. Hope, A. F. G. Wyatt, *Nature* **304**, 325 (1983).
11. F. R. Hope, M. J. Baird, A. F. G. Wyatt, *Phys. Rev. Lett.* **52**, 1528 (1984).
12. M. Brown and A. F. G. Wyatt, *J. Phys. Condens. Matter* **2**, 5025 (1990).
13. M. A. H. Tucker and A. F. G. Wyatt, *J. Low Temp. Phys.* **110**, 455 (1998).
14. When the cavity roton source was replaced by a single heater, there was no evidence for quantum evaporation signals from R^- rotons.
15. H. Baddar, D. O. Edwards, T. M. Levin, M. S. Pettersen, *Physica* B **194-6**, 513 (1994).
16. F. Dalfovo, A. Fracchetti, A. Lastri, L. Pitaevskii, S. Stringari, *Phys. Rev. Lett.* **75**, 2510 (1995).
17. C. E. Campbell, E. Krotscheck, M. Saarela, *ibid.* **80**, 2169 (1998).
18. M. B. Sobnack and J. C. Inkson, *Phys. Rev.* B **56**, R14271 (1997).

19. We thank the Engineering and Physical Sciences Research Council for financial support, M. Gear for making the apparatus, and C. D. H. Williams for advice on the electronic detection system. We benefited from general discussions with F. Dalfovo, M. Guilleumas, E. Krotscheck, M. B. Sobnack, S. Stringari, and C. D. H. Williams.

2 December 1998; accepted 18 January 1999

A Processive Single-Headed Motor: Kinesin Superfamily Protein KIF1A

Yasushi Okada and Nobutaka Hirokawa*

A single kinesin molecule can move "processively" along a microtubule for more than 1 micrometer before detaching from it. The prevailing explanation for this processive movement is the "walking model," which envisions that each of two motor domains (heads) of the kinesin molecule binds coordinately to the microtubule. This implies that each kinesin molecule must have two heads to "walk" and that a single-headed kinesin could not move processively. Here, a motor-domain construct of KIF1A, a single-headed kinesin superfamily protein, was shown to move processively along the microtubule for more than 1 micrometer. The movement along the microtubules was stochastic and fitted a biased Brownian-movement model.

A single kinesin molecule has two heads or motor domains (*1*) and moves processively (*2–4*), taking more than 100 steps before detaching from a microtubule (MT). The two-headed structure is assumed to be essential for processive movement, because engineered single-headed or monomeric molecules have motor activity but are not processive, whereas dimeric constructs have high processivity (*4–9*). The prevailing hypothesis for the mechanism of processive movement is the "walking model" (*2, 10*), in which one head anchors the molecule to the MT while the other moves to the next binding site on the MT. Thus, a single-headed molecule is not expected to move processively because the molecule is not anchored while it moves to the next binding site.

A monomeric kinesin superfamily protein, KIF1A, which has only one motor domain, supports MT gliding at ~1.2 μm/s (*11*). It remains unresolved whether this naturally single-headed KIF is processive or not. A conventional, very low motor density MT gliding assay and a single-motor motility assay with fluorescently labeled full-length KIF1A protein suggested that it is processive (*12*). However, the results were very variable, possibly because of the instability or heterogeneity of the full-length KIF1A recombinant protein. Thus, to overcome these problems, we produced a KIF1A motor-domain chimer-

Department of Cell Biology and Anatomy, Graduate School of Medicine, University of Tokyo, Hongo, Tokyo 113-0033, Japan.

*To whom correspondence should be addressed. E-mail: hirokawa@m.u-tokyo.ac.jp

ic construct, C351, for further analysis.

The design of C351 is based on the shortest monomeric motile, but nonprocessive, construct DmK351 made from *Drosophila* conventional kinesin (*4, 6*). The catalytic core of the conventional kinesin motor domain of K351 was swapped with that of KIF1A (*13*). Thus, C351 contains the catalytic core of the motor domain of KIF1A followed by the 23–amino acid "linker" of conventional kinesin (*14*), which is reported to be insufficient for dimerization (*8*). As a control, a dimeric conventional kinesin molecule, K381, was also constructed, containing the coiled-coil neck region essential for dimerization (*8, 15*).

The motor molecules were labeled with a red fluorescent dye, Alexa, and observed under a low background video-intensified microscope (*16*). When C351 molecules were applied at a relatively higher concentration (final 100 pM) in the presence of adenosine triphosphate (ATP, 2 mM), each of the MTs in the chamber was decorated with dozens of C351 molecules. They continuously moved to one end of the MT, and accumulated to create a bright spot (Fig. 1A). Almost all of the MTs (>99%) were strongly decorated only on one end. The other ends were either dimly or not at all decorated with C351. This lollipop-like decoration of the MTs was also observed with K381, as reported previously (*17*). In contrast, K351 did not bind to MTs even at 1000 pM in the presence of ATP, confirming the previous report that monomeric conventional kinesin does not show a processive movement in this type of assay (*4*).

At lower motor molecule concentrations (1 to 10 pM) of C351 or K381, MTs were sparsely decorated with several fluorescent spots (Fig. 1B), moving along them for several seconds. Statistical analysis of the fluorescence intensities of these moving spots indicated that they are single-motor molecules (Fig. 1C). Thus, under these conditions, we could observe the behavior of single-motor molecules (*18*).

Single C351 molecules were observed to move processively along MTs (Fig. 1B). To quantitatively measure the processivity of the movement (mechanical processivity), we plotted the exponential distribution of the duration of movement on the MT (*4, 19*). The best-fit curve indicated the mean duration of movement, or the time constant (τ_{mec}) of C351 dissociation from the MTs, to be 6.1 ± 0.8 s (Fig. 2A), suggesting the high processivity of a single-headed C351 motor, compared to 2.6 ± 0.2 s for K381 (Fig. 2B). The movement of single C351 molecules on the MTs was not smooth, and actually appeared oscillatory. Although it was on average unidirectional (Fig. 2D), single C351 motors sometimes paused for a while, or moved backward for a short distance, and then moved forward (arrowhead in Fig. 1B).

To quantitatively analyze this apparently oscillatory or fluctuating movement of C351, we plotted the distribution of the displacement (Fig. 2F). The plot fitted well with a normal distribution whose mean and variance increased linearly against time. The linear

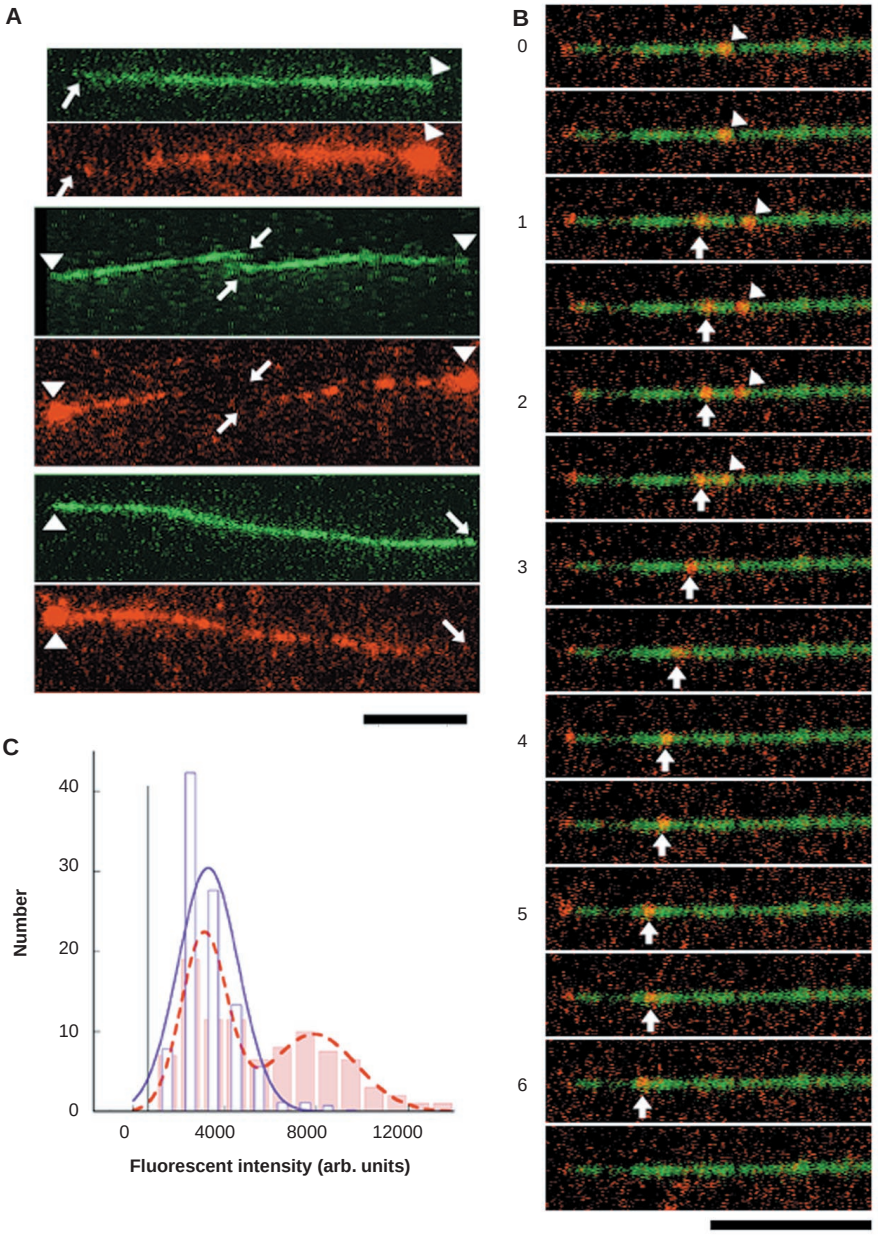

Fig. 1. Motility assay of fluorescently labeled C351. (**A**) High motor concentration assay of C351. C351 (red) was applied at 100 pM to MTs (green) fixed on a cover glass. The MTs were decorated with dozens of C351 molecules. The molecules moved continuously to one end of the MT (arrowhead) and accumulated at this end to create a bright spot. The other end was either dimly or not at all decorated with C351 (arrow). Scale bar, 2 μm. (**B**) Low motor density assay of C351. At 1 to 10 pM, MTs (green) were sparsely labeled with several fluorescence spots (red). The fluorescence intensity profile of these spots [see (C)] indicated that these spots were single C351 molecules. They attached to the MTs, moved along them for several seconds, and were finally detached from the MTs. Sometimes C351 moved backward (arrowhead), but it usually moved in one direction (arrow). Scale bar, 2 μm; frame interval, 0.5 s. (**C**) Intensity profile of the moving fluorescence spots. Blue (C351) and red (K381) bars show the measured distribution of the fluorescence intensities of C351 and K381 moving along the MTs. Blue and red lines show the theoretical curve assuming a Gaussian distribution. The variance was estimated from the observed values. The blue curve assumes that C351 is a monomer, and the red curve assumes that K381 is a dimer. The fluorochrome/protein ratio of the K381 used in this assay was 70%. Thus, 49% of the molecule is doubly labeled, and 42% is singly labeled, if the COOH-terminal cysteine residues are randomly labeled. These theoretical curves fit very well with the observed values, indicating that single fluorescent molecules are observed with our system, and that C351 is a monomer, whereas K381 is a dimer. A video illustrating motility data can be viewed at www.sciencemag.org/feature/data/985876.shl.

increase of the mean indicates the unidirectional constant-velocity movement on average. The linear increase of the variance cannot be explained by the error (or noise) in the position measurement. Such noise does not accumulate and is reflected as the constant term in the variance. The linear increase of the variance indicates the linear accumulation of random noise, as found in the Brownian movement. Thus, the distribution of the displacement of C351 suggests that it is a biased Brownian movement (that is, diffusion with a drift).

In contrast, K381 moved more smoothly in a single direction (Fig. 2E), as reported previously for the longer construct K440 (*4*). The distribution of its displacement fitted well with a normal distribution with a linearly increasing mean and a constant variance (Fig. 2G). This constant variance can be explained by the error in the position measurement. Thus, relative to C351, the movement of K381 is much smoother, as reported previously (*20*).

We further analyzed the movement of C351 and K381 by plotting the mean square displacement [MSD, $\rho(t)$] against time, which is a convenient quantitative measure of stochastic movement (*21*). The MSD plot of C351 (Fig. 2H) fitted very well with biased Brownian movement: $\rho(t) = 2Dt + v^2t^2$, where D is the diffusion coefficient and v is the (mean) velocity. The MSD plot of C351 fitted well with $D = 44{,}000 \pm 1200$ nm^2/s and $v = 140 \pm 10$ nm/s. This estimated value of D is much larger than the value expected from the fluctuation in the adenosine triphosphatase (ATPase) activity (<2400 nm^2/s) (*20*), whereas it is in good agreement with the value previously reported for one-dimensional Brownian movement in MT–motor protein systems (*22, 23*). In contrast, the MSD plot of K381 fitted well with $D = 2200 \pm 1000$ nm^2/s and $v = 710 \pm 10$ nm/s (Fig. 2H). These values are in good agreement with previous results ($D = 1400$ nm^2/s, $v = 670$ nm/s) (*20*), and the fluctuation of the movement of K381 can be explained by the fluctuation in the ATPase activity (*20*).

The difference between C351 and K381 in the degree of fluctuation of the movement is illustrated by the plot of the diffusion term, or $\rho(t) - v^2t^2$ (Fig. 2I). The movement of C351 is about 20 times as diffusive as that of K381. This heavily stochastic nature of the movement cannot be explained by the error of the position measurement, by the Brownian noise that often impedes the bead-based nanometry of the motor movement, or by any heterogeneity in the motor activity. The errors of the position measurement and the Brownian noise do not accumulate, and only contribute as the constant term to the diffusion term of MSD or the variance of the displacement. Furthermore, our single-motor assay is free from the Brownian noise because the position of the fluorescent spot directly reflects the position of the motor molecule. The heterogeneity in the motor activity would produce a variance that grew quadratically with time (*24*). Thus, the diffusive nature of the C351 movement would reflect its inherent nature rather than the artifactual noise.

With the single-motor motility assay, only active molecules that bind and move along MTs can be observed. To avoid this bias (*25*), we measured the kinetic parameters of the C351 ATPase, which reflect the mean enzymatic behavior of the population. As the kinetic index of processivity, we measured $k_{bi(ratio)}$, the ratio of the second-order rate constant of MT-activated ATPase activity ($k_{bi(ATPase)}$) and that of MT-activated adenosine diphosphate (ADP) release ($k_{bi(ADPrelease)}$), which indicates the number of ATPase cycles per motor-MT encounter (*26*).

The results of the kinetic assays are summarized in Table 1 (*27*). The kinetic proces-

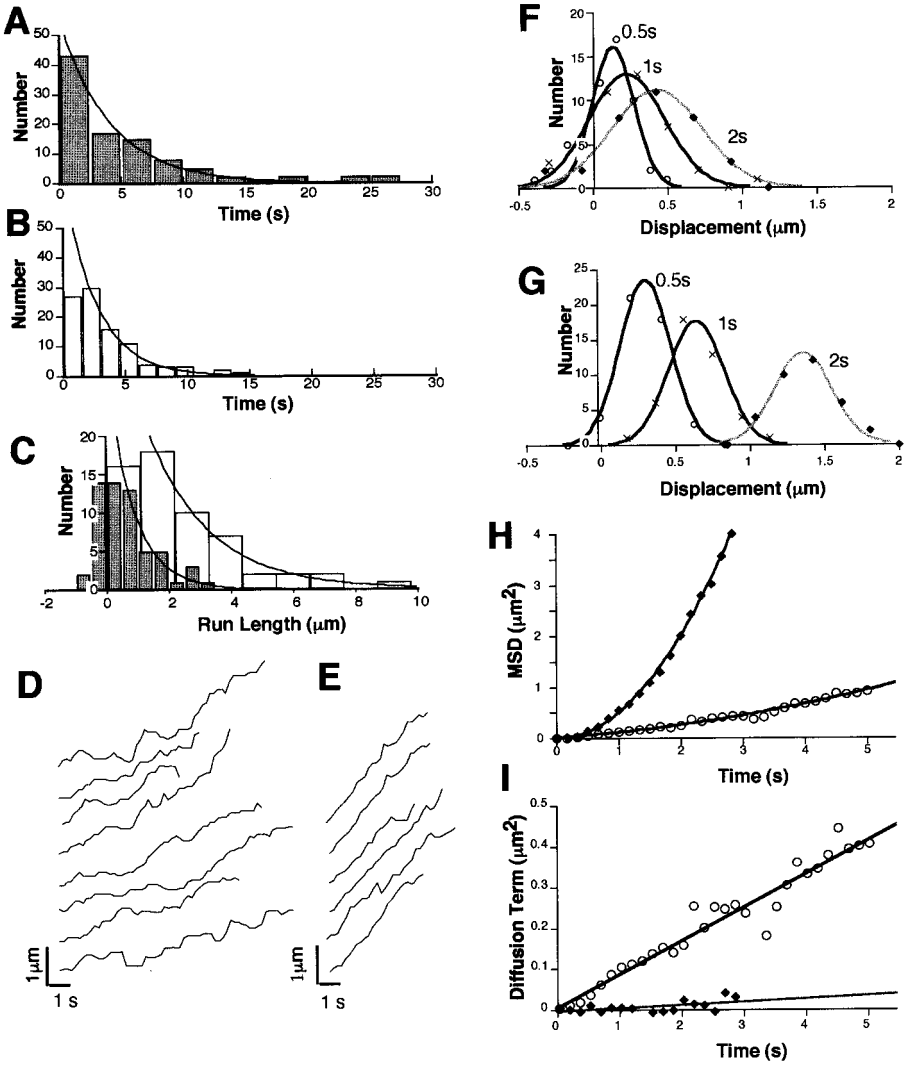

Fig. 2. Analysis of the movement of single fluorescently labeled C351 and K381 molecules. (**A** and **B**) Distribution of the duration of movement of motor C351 (A) and K381 (B). Bars show the measured values, and lines show the best fit with a single exponential distribution. The time constants τ_{mec} of the motor dissociation from MTs thus derived are 6.1 ± 0.8 s for C351 (A) and 2.6 ± 0.2 s for K381 (B). (**C**) Distribution of run length. Shaded bar indicates C351; open bar indicates K381. Curves show the best fits with a single exponential distribution, with $\mu = 0.84 \pm 0.2$ μm for C351 and 2.0 ± 0.2 μm for K381. (**D** and **E**) Typical traces of the displacement of the motor molecules (*39*). Each trace shows the path of an individual C351 (D) or K381 (E) motor. C351 movements are rather oscillatory or stochastic; K381 movements are smoother. (**F** and **G**) Distribution of the displacement of C351 (F) and K381 (G) plotted against time. Curves show the best fits with normal distributions ($\mu = 140$, 230, or 430 nm, $\sigma^2 = 4 \times 10^4$, 10×10^4, or 18×10^4 nm^2 for $T = 0.5$, 1, or 2 s, respectively, for C351; $\mu = 340$, 690, or 1400 nm, $\sigma^2 = 8 \times 10^4$ nm^2 for K381). (**H**) MSD, $\rho(t)$, of C351 (○) and K381(◆) plotted against time. Curves show the best fits with $\rho(t) = 2Dt + v^2t^2$ ($D = 44{,}000 \pm 1200$ nm^2/s, $v = 140 \pm 10$ nm/s for C351; $D = 2200 \pm 1000$ nm^2/s, $v = 710 \pm 10$ nm/s for K381). (**I**) The diffusion term or $\rho(t) - v^2t^2$ of C351 (○) and K381 (◆) plotted against time. Curves show the best fits with the same parameters as in (H).

sivity index $k_{bi(ratio)}$ of C351 was 690. On average, C351 hydrolyzes nearly 700 ATPs before detaching from the MT. This is more than five times the value for the dimeric kinesin K381, and more than 40 times that for the monomeric kinesin K351. This high kinetic processivity could be the source of the observed mechanical processivity. Dividing this value by the turnover rate k_{cat} (110 s^{-1}) yields a time constant for the motor-MT dissociation (τ_{kin}) of 6.3 s, showing good agreement with that obtained from the single-motor motility assay (τ_{mec} = 6.1 ± 0.8 s) (*28*). The agreement of τ_{kin} and τ_{mec} strongly suggests that the behavior of the fluorescent spots observed in the single-motor assays actually reflects the behavior of the single-motor molecules, and that the single-headed C351 is a highly processive motor. What, then, lends processivity to C351?

The kinetic processivity index $k_{bi(ratio)}$ is determined by the three kinetic parameters k_{cat}, $K^{0.5}_{MT(ATPase)}$, (MT concentration for half-saturation of ATPase) and $k_{bi(ADPrelease)}$. Among these, the $K^{0.5}_{MT(ATPase)}$ of C351 is smaller than that of K351 by a factor of about 100, whereas the other parameters differ in magnitude by a factor of only 2 to 3 (Table 1). Thus, the data suggest that C351 binds to the MT with exceptionally high affinity, so that more than several hundred ATPase cycles occur before it is detached from the MT.

The binding of C351 to MTs is very sensitive to the ionic strength (*29*), which suggests that it is mediated by electrostatic interactions, as proposed for kinesin (*4, 30*), whose positively charged residues might bind to the negatively charged region of tubulin (*31, 32*). Quite interestingly, a region just upstream of the well-conserved His-Ile-Pro-Tyr-Arg-Asp motif has six extra lysines in tandem (Fig. 3A). This region corresponds to loop 12 (*33*), which is suggested to be involved in MT-kinesin interactions (*32*). Thus, this loop with six extra lysines (which we call the "K-loop") is a good candidate to explain the exceptionally high affinity of KIF1A for the MT.

This speculation is supported by the following three results. First, molecular phylogenetic analysis demonstrates that the K-loop is conserved only in naturally monomeric KIFs (Unc104/KIF1 subfamily) but not in dimeric (or tetrameric) KIFs (Fig. 3A), indicating its unique role in monomeric KIFs. Second, a lysine hexamer (K_6) competitively inhibits the C351-MT interaction (Fig. 3B), with inhibition constant K_i = 80 nM. At 1 μM, K_6 completely blocks the binding to MTs by C351 in the single-motor assay. Third, a mutant C351 whose K-loop is replaced by the corresponding residues of kinesin showed less than one-fifth the affinity for the MT, and showed no binding to MTs in the single-motor assay (*34*). These results collectively suggest that this K-loop (and the MT region that binds to K_6) plays an essential role in the high-affinity binding of KIF1A to MTs.

Thus, C351 is anchored to the MT via the K-loop so as to prevent its diffusion away from the MT. At the same time, however, it should be able to translocate along the MTs, otherwise it cannot move because the motor domain is too

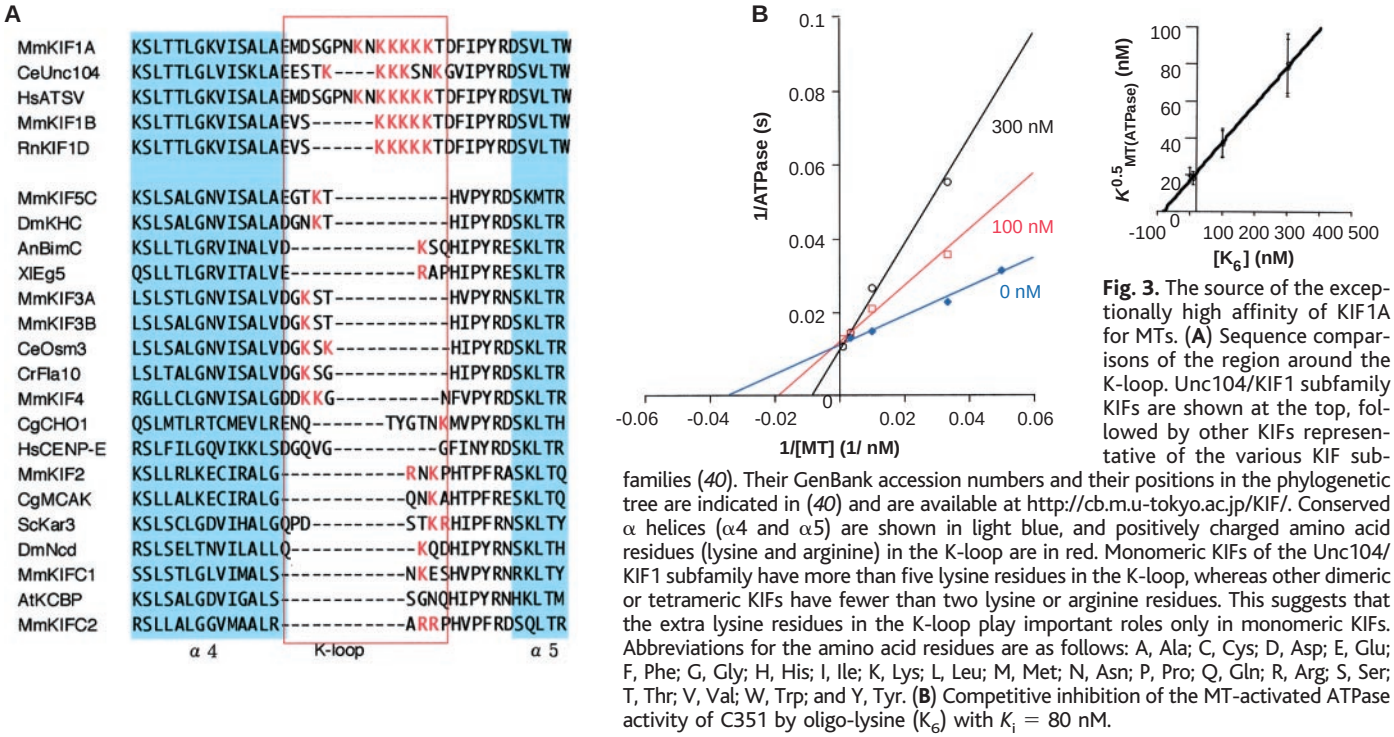

Fig. 3. The source of the exceptionally high affinity of KIF1A for MTs. (**A**) Sequence comparisons of the region around the K-loop. Unc104/KIF1 subfamily KIFs are shown at the top, followed by other KIFs representative of the various KIF subfamilies (*40*). Their GenBank accession numbers and their positions in the phylogenetic tree are indicated in (*40*) and are available at http://cb.m.u-tokyo.ac.jp/KIF/. Conserved α helices (α4 and α5) are shown in light blue, and positively charged amino acid residues (lysine and arginine) in the K-loop are in red. Monomeric KIFs of the Unc104/KIF1 subfamily have more than five lysine residues in the K-loop, whereas other dimeric or tetrameric KIFs have fewer than two lysine or arginine residues. This suggests that the extra lysine residues in the K-loop play important roles only in monomeric KIFs. Abbreviations for the amino acid residues are as follows: A, Ala; C, Cys; D, Asp; E, Glu; F, Phe; G, Gly; H, His; I, Ile; K, Lys; L, Leu; M, Met; N, Asn; P, Pro; Q, Gln; R, Arg; S, Ser; T, Thr; V, Val; W, Trp; and Y, Tyr. (**B**) Competitive inhibition of the MT-activated ATPase activity of C351 by oligo-lysine (K_6) with K_i = 80 nM.

Table 1. Summary of the mechanical and kinetic assays of the motor domain constructs. $s_{20,w}$, sedimentation coefficient; N.D., no detectable movement.

Construct	Hydrodynamic analysis		Single-motor motility assay		Kinetic assays					
	$s_{20,w}$ (S)	Oligomeric state	v (nm/s)	τ_{mec} (s)	k_{cat} (s^{-1})	$K^{0.5}_{MT(ATPase)}$ (nM)	$k_{bi(ATPase)}$ (s^{-1} μM^{-1})	$k_{bi(ADPrelease)}$ (s^{-1} μM^{-1})	$k_{bi(ratio)}$	τ_{kin} (s)
C351	3.4	Monomer	140	6.1 ± 0.8	110 ± 5	16 ± 8	6900	10 ± 3	690	6.3
K351	3.4	Monomer	N.D.	<0.27*	62 ± 3	1300 ± 400	48	3 ± 1	16	0.26
K381	5.1	Dimer	710	2.6 ± 0.2	64 ± 2	120 ± 40	530	4 ± 1	130	2.0

*Temporal resolution of our system (8/30 s).

small [~6 nm (*33, 35*)] to reach the next binding site, which is 8 nm away along the MT protofilament.

One possible model posits that extra binding sites exist on the MT and that the mechanical step size of C351 is smaller than that of conventional kinesin. Then, the small motor domain might be able to step to the next binding site. However, this model cannot explain the observed large fluctuation (variance = 400 nm^2 per ATPase cycle) compared with the small mean displacement (1.3 nm per ATPase cycle) (*36*).

Another possibility is that C351 moves by successive dissociation from and reassociation to the MT. This can explain the observed diffusive nature of the movement. However, after complete dissociation from the MT, the motor will rapidly diffuse away from it, and the probability of reassociation will be too low to explain the observed long movement. This difficulty can be overcome by assuming that C351 is weakly anchored to the MT so as not to diffuse away from it. That is, C351 is anchored to the MT in such a way that the electrostatic potential restricts its movement away from the MT while allowing free movement along the MT. This can be represented as a groove-shaped potential along the MT (*37*).

The free thermal fluctuation during this "weak binding state" enables C351 to move to the distant binding site, and also explains the highly fluctuating nature of the movement. When C351 switches to the strong binding state, it will bind to the "nearest" binding site. If there is a bias toward the plus-end direction in this rebinding step, this step can bias or rectify the thermal fluctuation in the weak binding state. This bias can be thermodynamically modeled as the anisotropy in the potential of interaction between C351 and the MT. This anisotropy might be produced by the periodic polarized nature of the MT protofilament (*38*), or by the structural change (or the "power stroke") in the motor domain. Similar bias toward the MT plus-end might also be produced in the dissociation step. When C351 makes a transition from the strong to the weak binding state, there might be some structural change in the motor domain, which pushes C351 toward the MT plus-end (Fig. 4). This model fits very well to the observed movement of C351 with parameters of reasonable values (*38*).

In this model, the thermal diffusion in the weak binding state is essential for the movement. The presumable structural changes in the motor (power stroke) or the anisotropy in the potential of the motor-MT interaction by themselves are too small to move the motor to the next binding site. The thermal diffusion allows the motor to reach the next binding site. The power stroke, or the anisotropy in the potential, only biases or rectifies the undirected thermal diffusion toward the MT plus-end. That is, this model envisions that the ATPase hydrolysis is used for the rectification of the thermal diffusion by the transition of the binding state or the structural changes in the motor.

In a conventional MT gliding assay, binding of other motor molecules on the glass surface anchors the whole system to the MT, and only a small fluctuation within the reach of the motor-glass linker is allowed. This can effectively reduce the possibility of the backward movement if the reach is short enough. This will enable rapid movement with less fluctuation. This mechanism might explain the discrepancy between the motile behavior of C351 in the multiple-motor assay (smooth unidirectional movement at 1.2 μm/s) and in the single-motor assay (biased Brownian movement at 0.14 μm/s).

The combination of the single-motor motility assay and the biochemical assay has conclusively demonstrated the processivity of the monomeric KIF1A motor-domain construct C351. The kinetic measurements sug-

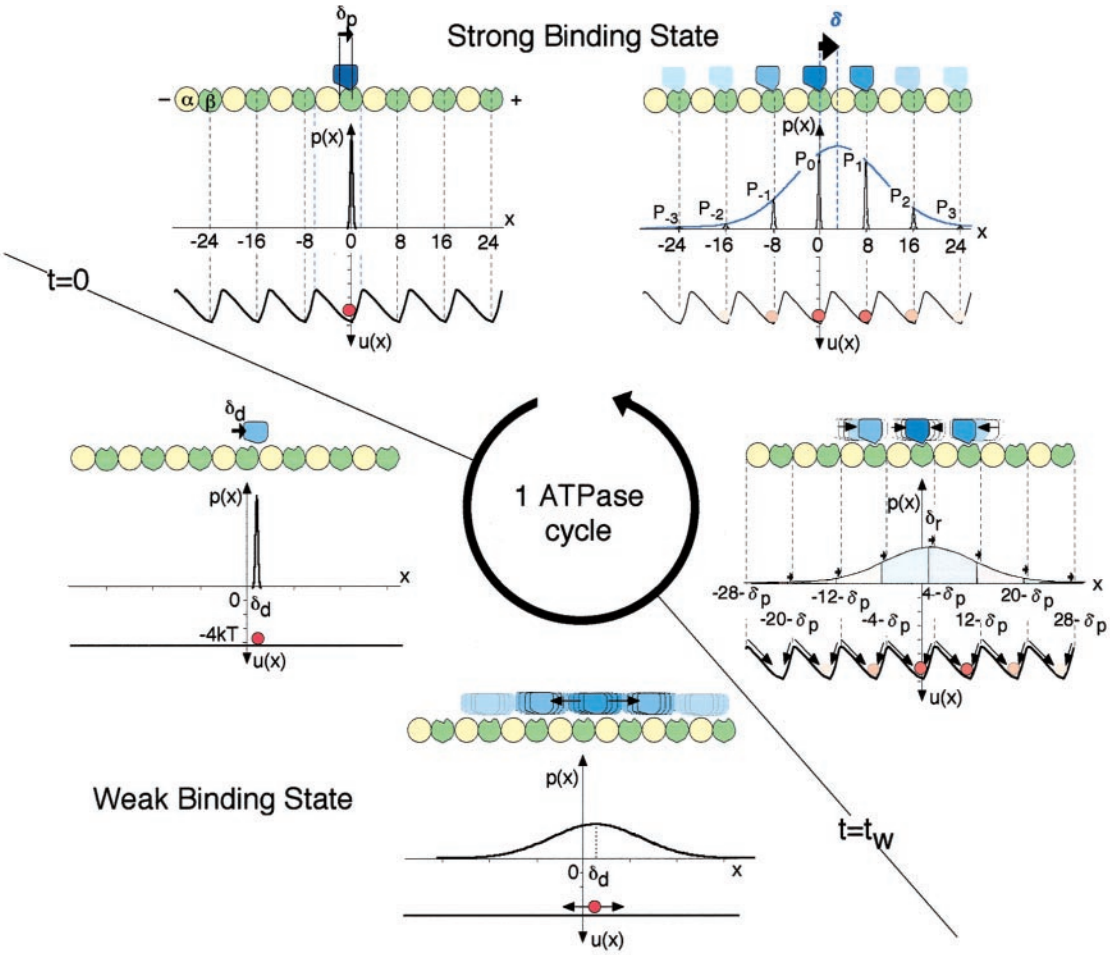

Fig. 4. Model of the processive movement of monomeric C351. Each panel consists of three parts. At the top is a schematic representation of C351 and a MT protofilament (yellow and green depict α tubulin and β tubulin, respectively). The middle and bottom parts show the probability distribution $p(x)$ of the position of C351, and the potential $u(x)$, respectively (*38*).

gest the source for this high processivity, whereas the single-motor assay demonstrates the diffusive nature of its movement. These results suggest a new model for kinesin movement. Future studies must be carried out to test these hypotheses.

References and Notes

1. N. Hirokawa *et al*., *Cell* **56**, 867 (1989); J. M. Scholey, J. Heuser, J. T. Yang, L. S. Goldstein, *Nature* **338**, 355 (1989).
2. J. Howard, A. J. Hudspeth, R. D. Vale, *Nature* **342**, 154 (1989).
3. S. M. Block, L. S. Goldstein, B. J. Schnapp, *ibid*. **348**, 348 (1990).
4. R. D. Vale *et al*., *ibid*. **380**, 451 (1996).
5. E. Berliner, E. C. Young, K. Anderson, H. K. Mahtani, J. Gelles, *ibid*. **373**, 718 (1995).
6. Y. Inoue *et al*., *Proc. Natl. Acad. Sci. U.S.A.* **94**, 7275 (1997).
7. W. O. Hancock and J. Howard, *J. Cell Biol.* **140**, 1395 (1998).
8. W. Jiang, M. F. Stock, X. Li, D. D. Hackney, *J. Biol. Chem.* **272**, 7626 (1997).
9. W. Jiang and D. D. Hackney, *ibid.*, p. 5616; Y. Z. Ma and E. W. Taylor, *ibid.*, p. 717; S. P. Gilbert, M. L. Moyer, K. A. Johnson, *Biochemistry* **37**, 792 (1998).
10. B. J. Schnapp, B. Crise, M. P. Sheetz, T. S. Reese, S. Khan, *Proc. Natl. Acad. Sci. U.S.A.* **87**, 10053 (1990); D. D. Hackney, *ibid.* **91**, 6865 (1994); Y. Z. Ma and E. W. Taylor, *J. Biol. Chem.* **272**, 724 (1997).
11. Y. Okada, H. Yamazaki, A. Y. Sekine, N. Hirokawa, *Cell* **81**, 769 (1995).
12. Provided as supplementary material at www.sciencemag.org/feature/data/985876.shl.
13. Simply deleting the COOH-terminal residues of KIF1A did not produce a fully active, stable protein. Addition of the 23–amino acid "linker" of conventional kinesin, however, greatly improved the stability of the KIF1A motor-domain construct. From a murine conventional kinesin KIF5C, we made the construct K351, which corresponds to DmK351, a widely used monomeric construct. Then, its first 329 amino acids (from the first methionine to the middle of α6, the last α helix in the catalytic core) was swapped with the corresponding residues (1 to 356) of KIF1A. As a control, a dimeric molecule, K381, a murine version of DmK381, was also constructed, which contains the coiled-coil neck region essential for dimerization (*8, 15*). To the COOH-termini of these three constructs, we added a $(His)_6$ tag for purification and a reactive cysteine residue for labeling. These constructs were expressed with the pET expression system (Novagen) in *Escherichia coli*. Bacterially expressed proteins were purified by immobilized metal affinity chromatography and labeled with Alexa-594 maleimide (Molecular Probes) at a fluorochrome/protein ratio of 0.7 to 0.9.
14. There is a lack of consensus with regard to the terminology of the domains of kinesin, or KIFs. Here, we refer to the region from β1 to α6 as the "catalytic core" region, the following region before α7 as the "linker," and the first coiled-coil α7 (the essential domain for the dimerization) as the "neck."
15. S. Sack *et al*., *Biochemistry* **36**, 16155 (1997); B. Tripet, R. D. Vale, R. S. Hodges, *J. Biol. Chem.* **272**, 8946 (1997).
16. T. Funatsu, Y. Harada, M. Tokunaga, K. Saito, T. Yanagida, *Nature* **374**, 555 (1995); M. Tokunaga, K. Kitamura, K. Saito, A. H. Iwane, T. Yanagida, *Biochem. Biophys. Res. Commun.* **235**, 47 (1997). Motor proteins were labeled with Alexa 594 C5-maleimide (Molecular Probes), and MTs were labeled with Bodipy-FL (Molecular Probes). Alexa 594 was selected because of its high photostability, large Stokes shift, high extinction coefficient, and high quantum yield. Motor proteins were filtered through ultrafiltration membranes just before use to remove aggregates. The filtrate was immediately diluted with motility buffer [50 mM imidazole, 5 mM Mg-acetate, 1 mM EGTA, 50 mM K-acetate, 10 mM dithiothreitol, 0.1% Triton X-100, casein (1 mg/ml), 2 mM ATP, and 10 μM paclitaxel] containing an oxygen scavenger system [1% glucose, glucose oxidase (0.05 mg/ml), and catalase (0.1 mg/ml)] [Y. Harada, K. Sakurada, T. Aoki, D. D. Thomas, T. Yanagida, *J. Mol. Biol.* **216**, 49 (1990)]. The temperature of the specimen stage was controlled at 26° ± 1°C by the air conditioner of the clean room. Epifluorescent images were observed under an Olympus BX microscope with a PlanApo 100×/1.40 objective lens and filter sets suited to Bodipy and Alexa (Olympus). Any part not necessary for the epifluorescent imaging was removed. An excitation beam passed through the sample was projected to the wall of the room so as not to cause reflection back into the light path of the emitted fluorescence. These improvements effectively reduced the background noise level (Fig. 1C) below the fluorescence signals of single Alexa molecules. The fluorescence images were projected to a Gen IV image-intensified cooled charge-coupled device camera (V/ICCD, Princeton Instruments) and electronically amplified with an image processor (Argus-10, Hamamatsu Photonics, Japan). The images were integrated for eight frames to improve the signal/noise ratio. Thus, the spatial and temporal resolution of this system is 50 nm (= pixel size) and 8/30 s, respectively. The resultant images were further analyzed on a Macintosh computer using the public-domain program NIH Image (available at http://rsb.info.nih.gov/nih-image/) with a custom macro program for semi-automatic quantification of fluorescent intensity and displacement.
17. R. B. Case, D. W. Pierce, B. N. Hom, C. L. Hart, R. D. Vale, *Cell* **90**, 959 (1997).
18. The combination of a photostable, bright dye (Alexa) and the oxygen scavenger system reduced the photobleaching rate to $<1/30\ s^{-1}$, so that we can almost neglect the effect of photobleaching in the motility assays.
19. Previous reports on the single-motor assay of conventional kinesin (*4*) use mean run-length of the motor as the index of the mechanical processivity. However, this parameter is sensitively affected by the occasional backward movement. Therefore, it is not suitable for C351 as shown in Fig. 2C.
20. K. Svoboda, P. P. Mitra, S. M. Block, *Proc. Natl. Acad. Sci. U.S.A.* **91**, 11782 (1994).
21. S. Chandrasekhar, *Rev. Mod. Phys.* **15**, 1 (1943).
22. R. D. Vale, D. R. Soll, I. R. Gibbons, *Cell* **59**, 915 (1989).
23. T. Nakata, Y. R. Sato, Y. Okada, Y. Noda, N. Hirokawa, *Biophys. J.* **65**, 2504 (1993); Y. Imafuku, Y. Y. Toyoshima, K. Tawada, *ibid*. **70**, 878 (1996).
24. M. J. Schnitzer and S. M. Block, *Nature* **388**, 386 (1997).
25. For example, there is a possibility that only a minor population of aggregate or illegitimate dimers were observed to move, though this possibility is almost negligible from the hydrodynamic analysis (K_{diss} for dimerization is >1 μM, whereas the assays were performed at <10 pM) and the fluorescent intensity distribution of C351 (Fig. 1C). However, there still remains a possibility that the fluorescent labeling might have affected the dimerization and that non-fluorescent C351 might preferentially associate with fluorescently labeled molecules.
26. D. D. Hackney, *Nature* **377**, 448 (1995).
27. MT-activated ATPase activity was assayed with the EnzChek phosphate assay kit (Molecular Probes). MT-activated ADP release was measured by the method of Hackney (*8, 9, 26*). The reactions were performed in the motility buffer without the oxygen scavenger system, and all assays were performed at 26° ± 1°C.
28. The kinetic parameters of Alexa-labeled C351 were also measured to assess the effects of fluorescent labeling. The parameters of Alexa-labeled C351 were not different from those of unlabeled C351, which effectively excludes the possibility that Alexa labeling changed the behavior of C351.
29. The addition of 50 mM K-acetate (final K-acetate concentration = 100 mM) completely blocks the binding of C351 to MTs in the single-motor assay. In the same buffer, $K^{0.5}_{MT(ATPase)}$ was >200 nM, indicating that the affinity of C351 for MTs was reduced by a factor of 10.
30. S. P. Gilbert, M. R. Webb, M. Brune, K. A. Johnson, *Nature* **373**, 671 (1995); Y. Z. Ma and E. W. Taylor, *Biochemistry* **34**, 13242 (1995).
31. C. Tucker and L. Goldstein, *J. Biol. Chem.* **272**, 9481 (1997).
32. G. Woehlke *et al*., *Cell* **90**, 207 (1997); M. C. Alonso, J. van Damme, J. Vandekerckhove, R. A. Cross, *EMBO J.* **17**, 945 (1998).
33. F. J. Kull, E. P. Sablin, R. Lau, R. J. Fletterick, R. D. Vale, *Nature* **380**, 550 (1996).
34. The K-loop of C351 (residues 288 to 303) was replaced with the corresponding region of K351 (residues 272 to 276). This replacement did not affect the k_{cat} of MT-activated ATPase, but the $K^{0.5}_{MT(ATPase)}$ value was more than five times that of C351. In the single-motor assay, this mutant showed no binding to MTs, hence no processive movement was observed.
35. F. Kozielski *et al*., *Cell* **91**, 985 (1997).
36. If each ATPase cycle produces N mechanical steps, the displacement per mechanical step should distribute roughly between $(1.4/N) - [1.5(400/1.3)^{1/2}/N^{1/2}]$ and $(1.4/N) + [1.5(400/1.3)^{1/2}/N^{1/2}]$. To encompass this displacement by a 6-nm motor, N should be >20, which gives a mean mechanical step size of 0.065 nm, smaller than the size of the atom. Other models, such as a loose-coupling model with constant mechanical step size and fluctuating coupling ratio (N), also give subatomic step size.
37. From thermodynamics theory, the observed kinetic or mechanical parameters collectively give the difference between C351 and K381 in the depth of the potential as ~$4kT$, where T is the absolute temperature and k is the Boltzmann constant. The extra lysines in the K-loop would make this difference in the binding energy.
38. As discussed in the supplementary material (*12*), three biases (the anisotropy of the potential δ_p, the power stroke in the rebinding step δ_r, and the power stroke in the dissociation step δ_d) additively work as the net bias per each chemical cycle ($\delta = \delta_p + \delta_r + \delta_d$). The thermal diffusion in the weak binding state (duration t_w) reflects the heavily stochastic nature of the movement. Thus, this model gives the mean velocity and the apparent diffusion coefficient of C351 as $v = 100\delta$ nm/s and $D = 100D_w t_w$ nm²/s, where D_w is the diffusion coefficient. The observed value yields estimates of $v = 140$ nm/s and $D = 44{,}000$ nm²/s. Hence, $\delta = 1.4$ nm and $D_w \cong 10^{-9}$ cm²/s, assuming that t_w is several milliseconds (*8*). The D_w value is in good agreement with the diffusion coefficient of protein freely moving along a linear substrate (*23*). The δ value also agrees with the structurally estimated values. The size of the power stroke (δ_r or δ_d) would be <2 nm, and the structural data on the position of the kinesin-MT binding [L. A. Amos and K. Hirose, *Curr. Opin. Cell Biol.* **9**, 4 (1997)] suggest that $\delta_p \cong 1$ to 2 nm. Thus, this model can quantitatively explain the observed biased Brownian movement of C351 with parameters of reasonable values.
39. The displacement of the ith fluorescent spot at time t [$d_i(t)$] was calculated as $d_i(t) = [\mathbf{x}_i(t) - \mathbf{x}_i(0)]\cdot\mathbf{e}_i$, where $\mathbf{x}_i(t)$ and $\mathbf{e}_i$ are the position of the centroid of the fluorescent spot at time t, and the unit vector of the orientation of the MT along which the fluorescent spot moves, respectively. Plots of $d_1(t)$, $d_2(t)$, $d_3(t)$, . . . against t are shown in Fig. 2, D and E, and the distribution of $d_i(0)$, $d_i(0.5)$, $d_i(1)$, and $d_i(2)$ are shown in Fig. 2, F and G. The MSD [$\rho(t)$] was calculated as $\rho(t) = \{\Sigma_i[d_i(t)]^2\}/\Sigma_i(1)$ and was plotted against t in Fig. 2H. In Fig. 2I, $\rho(t) - v^2t^2$ is plotted against t, where v is the mean velocity estimated by fitting $\rho(t)$ with $\rho(t) = 2Dt + v^2t^2$.
40. N. Hirokawa, *Science* **279**, 519 (1998).

41. Supported by a Center of Excellence grant-in-aid from the Ministry of Education, Science, Sports, and Culture of Japan (N.H.). We thank K. Abe for his technical assistance with the microscopy system, H. Sato and H. Fukuda for their secretarial assistance, M. Sugaya for her technical assistance, and M. Kikuchi, M. Kikkawa, and other members of our lab for discussions and suggestions.

13 October 1998; accepted 13 January 1999